ISSN 0915-633X

NATIONAL INSTITUTE FOR FUSION SCIENCE

Vortical Structure of Turbulence

S. Kida

(Received - Oct. 19, 2000)

NIFS-666 Nov.2000

RESEARCH REPORT
NIFS Series

TOKI, JAPAN

Vortical Structure of Turbulence

Shigeo KIDA

Theory and Computer Simulation Center,
National Institute for Fusion Science,
Oroshi-cho 322-6, Gifu, 509-5292

The vortical structure of isotropic turbulence is analyzed by the use of the low-pressure-vortex visualization method. It is found that every swirling vortex tube is accompanied with winding vortex layers around it. The vorticity in these layers is perpendicular to the vortex tube. The Reynolds number dependence of the contribution of the vortex tubes to various physical quantities is investigated.

KEYWORDS: Low-pressure vortex, turbulence

1 Introduction

Thanks to the highly-developed (and still developing) computer science the detailed analysis of the vortical structure of turbulence has become possible. It is extremely helpful for the understanding of such a complicated phenomenon as turbulence to observe by our own eyes what is actually going on. This may lead to get a new insight on turbulence, to develop a new technique of control of turbulence, and so on.

However, there seems no perfect visualization method to describe a time-dependent three-dimensional vector field with complicated structure. We try in this paper to capture some aspects of turbulent flow structures by making use of the low-pressure-vortex visualization method which we have developed recently [?, ?, ?, ?, ?]. We analyze a numerically simulated box turbulence, the method of simulation and the resulting flow characteristics are described in §2. The analysis is made by a perspective representation of vortex axes and cores in §3 and by taking a cross-section of a vortex in §4. Various statistics including the mean radius and the circulation of vortex cores, and the Reynolds number dependence of core characteristics, are discussed in §5. Finally, concluding remarks are made in §6.

2 Forced Isotropic Turbulence

For the purpose of detailed analysis of the vortical structure, it is preferable to take the simplest possible flow, which is the isotropic turbulence. We consider an incompressible flow in a periodic cube of side 2π which is governed by the Navier-Stokes equation,

$$\frac{\partial}{\partial t}\boldsymbol{u} + (\boldsymbol{u}\cdot\nabla)\boldsymbol{u} = -\frac{1}{\rho}\nabla p + \nu\nabla^2\boldsymbol{u} + \boldsymbol{f}\ , \quad (1)$$

and the continuity equation,

$$\nabla\cdot\boldsymbol{u} = 0, \quad (2)$$

where $\boldsymbol{u}(\boldsymbol{x},t)$ is the velocity, $\boldsymbol{x}$ is the space coordinate, t is the time, ρ is the constant density, p is the pressure, ν is the kinematic viscosity, and $\boldsymbol{f}$ is an external force.

Talbe 1. Characteristic quantities of forced turbulence. $N^3 = 512^3$, $\Delta x = 0.012$, $\Delta t = 0.00125$.

ν	Re	R_λ	$\mathcal{E}$	Q	ϵ	λ	l_K	$k_\mathrm{max}/k_\mathrm{K}$
2.5×10^{-3}	1210	86	0.55	21.6	0.10	0.36	0.020	5.1
1.25×10^{-3}	2363	119	0.57	44.5	0.11	0.25	0.011	2.8
0.625×10^{-3}	4181	170	0.56	93.0	0.12	0.17	0.007	1.7

These equations are solved numerically by the spectral method after the velocity field is expanded into the Fourier series as $\boldsymbol{u} = \sum \tilde{\boldsymbol{u}} \exp[i\boldsymbol{k}\cdot\boldsymbol{x}]$, where the number of Fourier modes is N^3. The aliasing interaction is eliminated by a grid shift/octodecahedron cutoff. The time integration is performed by the fourth-order Runge-Kutta scheme. The forcing is imposed to maintain the turbulence statistically stationary, which is useful to obtain statistics of high quality by time averaging. In order to minimize contamination effects of the forcing to the small-scale motions which we are currently interested in, the forcing should be limited to the large scales. In the present simulation the amplitudes of the Fourier coefficients of the velocity field at low wavenumbers ($|\boldsymbol{k}| < 2.5$) are kept constant at all the time, whereas the phases are allowed to change according to the governing equations (1) and (2).

The numerical parameters N, ν and Δt must be set up carefully to guarantee the numerical accuracy. For a given N (which is limited by the computer power) and a forcing amplitude, the viscosity ν should be above some threshold so that the cutoff wavenumber $k_\mathrm{max} = \frac{1}{2}N$ may be larger than some multiple (say, 1.5) of the Kolmogorov wavenumber $k_K = (\epsilon/\nu^3)^{1/4}$, where ϵ is the mean energy dissipation rate. The time step width Δt is limited by the CFL condition which depends on the grid width $\Delta x = 2\pi/N$. These values are determined a posteriori after trial and error. In the present case we found $\nu = 0.625 \times 10^{-3}$ and $\Delta t = 0.00125$ as acceptable lower limits for $N = 512$. Furthermore, in order to realize a statistically stationary turbulence which is independent of the initial condition, the simulation should be run for quite a long time. The characteristic time of energy-containing eddies may be estimated as $\mathcal{E}/\epsilon$ (eddy-turnover time, say), where $\mathcal{E} = \frac{1}{2}\langle|\boldsymbol{u}|^2\rangle$ is the kinetic energy of turbulence and $\langle\ \rangle$ denotes the spatial average. The velocity fields we analyze here were taken after several eddy-turnover times.

The Reynolds number dependence of the vortical structure is examined by comparing three cases of different (by factors 2 and 4) viscosity. The length-scale and the velocity-scale of energy-containing eddies may be estimated as $\mathcal{E}^{3/2}/\epsilon$ and $\mathcal{E}^{1/2}$, respectively. The Reynolds number is then defined by $Re = \mathcal{E}^2/\nu\epsilon$. The micro-scale Reynolds number based on the Taylor length λ is written as $R_\lambda = u'\lambda/\nu$, where u' is the rms value of a single component of the velocity.

Some of global characteristic quantities in the present numerical turbulence are listed in table 1. The kinetic energy $\mathcal{E}$ and the dissipation rate ϵ are nearly independent of the viscosity, the enstrophy $Q = \langle|\boldsymbol{\omega}|^2\rangle$ and the Reynolds number Re are inversely proportional to ν. The micro-scale Reynolds number, the Taylor length and the Kolmogorov length $l_K = (\nu^3/\epsilon)^{1/4}$ vary roughly as $R_\lambda \propto Re^{1/2}$, $\lambda \propto Re^{-1/2}$ and $l_K \propto Re^{-3/4}$, respectively. All of these Reynolds number dependences are consistent with the classical universal equilibrium theory by Kolmogorov. The characteristic time (eddy-turnover time) is $\mathcal{E}/\epsilon = 5.5, 5.2, 4.7$, while that of the small-scale motion (the Kolmogorov time)

is $(l_K^2/\epsilon)^{1/3} = 0.16, 0.10, 0.07$ for the three cases. The time step width $\Delta t = 0.00125$ is sufficiently smaller than these values. The cutoff wavenumber is greater than the Kolmogorov wavenumber times a commonly accepted tolerable factor (≈ 1.5). Therefore we may say that small scale motions are well resolved. [1]

3 Visualization of Flow Field

Many visualization techniques have been developed so far in order to understand the structure of the flow field. All kinds of field quantities available, which include not only the velocity and pressure fields but also a variety of quantities derived by taking their spatial derivatives and combining them, are employed. The representation methods are also variegated. Vector lines with and without arrows, isosurfaces, scattered points are combined with various colors on them. Each representation captures different aspects of flow fields but can never be said to be perfect. It may be fruitful to compare different methods and use them complementally.

Here, we analyze the vortical structure by the low-pressure-vortex visualization method [3, 4, 5, 7]. This method is based on the pressure field. The idea is that the pressure around the center of a swirling tubular vortex tends to be lower than the surroundings. We search numerically the local minimum (in two-dimensional sense) lines of pressure in the whole flow field. They spread and stretch all over the flow like nets of roots. By definition the pressure takes a local minimum on a plane perpendicular to the minimum lines. In most cases there are swirling motions around the lines, but exceptions of

(a)

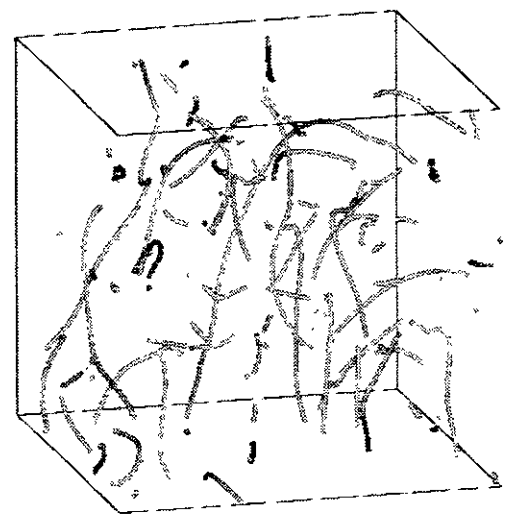

(b)

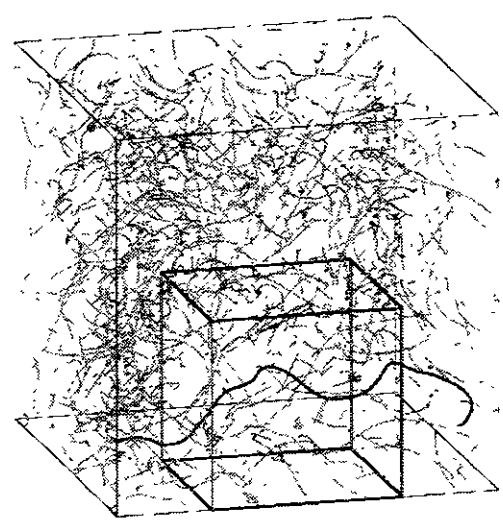

Figure 1: Axes of low-pressure vortices. (a) $R_\lambda = 86$ and (b) $R_\lambda = 170$. The cubes shown here are 1/64 of the whole simulation domain. The small cube in (b), the side of which is half of the large one, is magnified in figure 2 below.

[1] A simulation with even smaller viscosity 0.3125×10^{-3} ran without numerical blow-up, but the vorticity field was under-resolved.

(a)

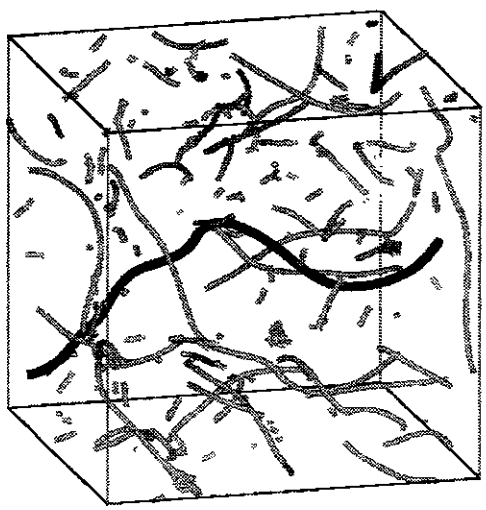

(b)

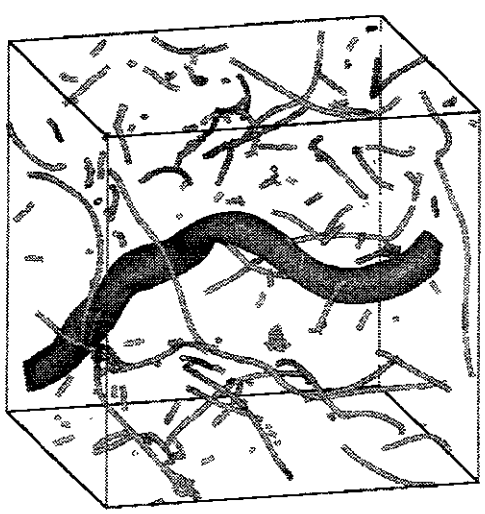

Figure 2: Axes of low-pressure vortices. $R_\lambda = 170$. A 1/256 of the whole simulation box (or the small box in figure 1(b)) is shown. A particular vortex axis is highlighted in (a) and its core is drawn in (b).

(a)

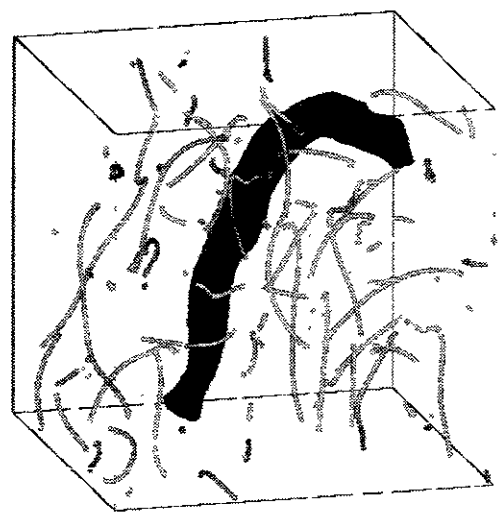

(b)

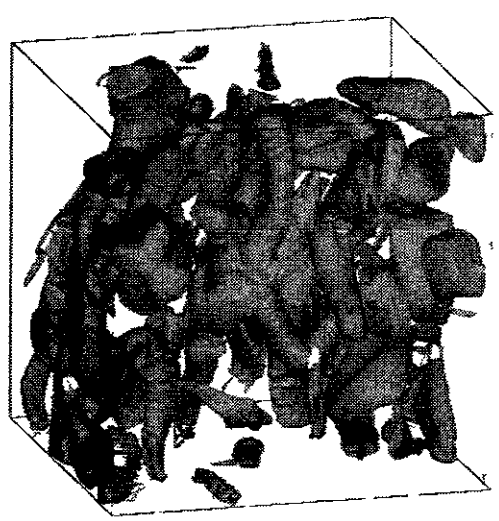

Figure 3: Vortex core. (a) A single vortex. (b) All the vortices. $R_\lambda = 86$.

$10 \sim 20$ % also. Since we are interested in tubular swirling vortices, we take only those lines that have swirling motions around them [5]. In the vicinity of minimum lines there is always a radially concave tubular region of pressure ($\partial^2 p/\partial r^2 > 0$), where r is the radial variable. Thus, a tubular region associated with every minimum line can be clearly defined as bounded by the inflection surface ($\partial^2 p/\partial r^2 = 0$). This object of cylindrical topology, which we have named the *low-pressure vortex*, is used as the reference to analyze the flow structure. The minimum line and the concave region of pressure are called the *axis* and *core* of the low-pressure vortex, respectively.

The axes of low-pressure vortices educed numerically are drawn in figure 1 for (a) $R_\lambda = 86$ and (b) $R_\lambda = 170$. Here, only a 1/64 of the whole flow field is shown for better appearance. The side of the cubes (which are composed of 128^3 grid points) is 4.4λ and 9.2λ. That is, the box (a) is about a half of (b) in the unit of λ.

The small box in figure 1(b) is enlarged by factor 2 in figure 2. Now the number density of the axes looks comparable between figure 1(a) and figure 2. This suggests that the mean distance between axes may scale with λ.

As described above, the extent of the low-pressure vortex is bounded by clearly defined inflection surfaces of the pressure field. Since the positions of the surfaces are stored, the contributions of vortex cores to various physical quantities including the core volume can easily be calculated (see §5). In figure 3, we plot the periphery of the vortex cores for (a) a particular vortex and (b) for all the vortices in this box in the case of $R_\lambda = 86$. The mean core radius is $7.8 l_K$ and they occupy 26% of the total volume. Figure 2 is a similar plot for $R_\lambda = 170$.

4 Structure of Cross-section

A tubular vortex has a strong vorticity along it. It induces a swirling motion which wraps the surrounding vorticity around it to generate spiral vortex layers. The direction of vorticity in the spirals is orthogonal to the vortex tube. This spiral was first derived as an exact solution of the Navier-Stokes equation by Moore [8] around a decaying straight vortex tubes (Oseen's vortex) in a simple shear in the special case that the directions of the vortex tube and the simple shear are parallel. In general cases that the two directions are not parallel, the surrounding vortices are wrapped, tilted and stretched around the tube [2].

In figure 5, we plot various fields on a cross-section of a vortex shown by a panel in figure 4. The side of the square is $40\Delta x$ ($= 24 l_K = 1.3\lambda$). The vortex axis is located on the center. In the contour plots the values are larger in darker areas. Figures (a), (b) and (c) are contours of the magnitude of

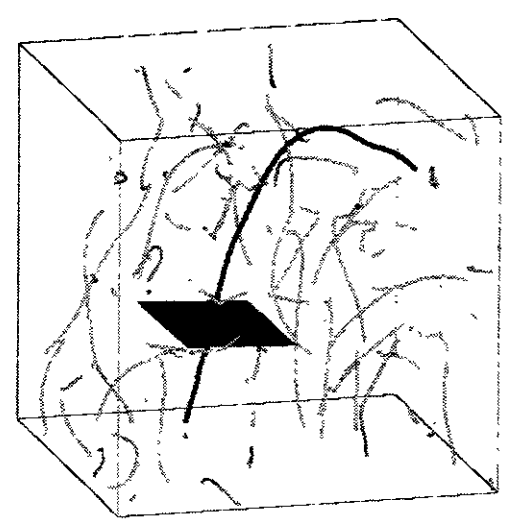

Figure 4: A particular vortex axis and a square panel across it. Various field quantities on this panel are drawn in figure 5

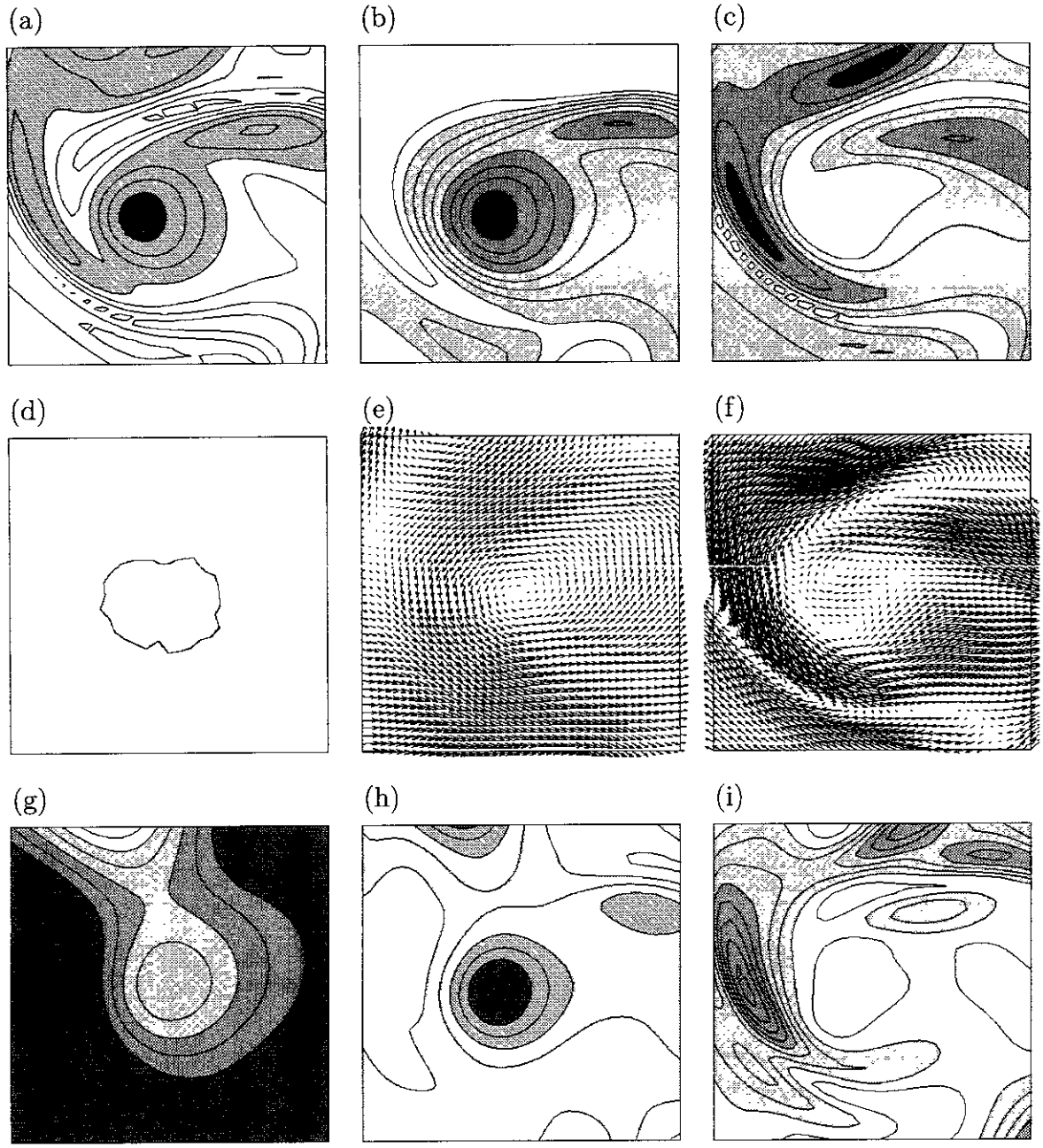

Figure 5: Cross-sectional fields on the plane shown in figure 4. (a) Vorticity magnitude. (b) Axial vorticity. (c) Cross-axial vorticity magnitude. (d) Core periphery. (e) Cross-axial velocity relative to the axis. (f) Cross-axial vorticity vector. (g) Pressure. (h) Laplacian of pressure. (i) Energy dissipation rate. The side of the square is $40\Delta x$ ($= 24l_K = 1.3\lambda$). The axis is located at the center. The values are larger at darker areas. $R_\lambda = 86$.

Talbe 2. Core statistics

R_λ	$V_{\rm core}/V$	$Q_{\rm core}/Q$	$\epsilon_{\rm core}/\epsilon$	$\omega_\parallel/\sqrt{Q}$	$R_{\rm core}/l_{\rm K}$	Γ/ν
86	0.22	0.46	0.19	2.58	7.8	84
119	0.16	0.39	0.14	2.64	6.3	57
171	0.13	0.36	0.14	2.72	4.3	35

vorticity, the axial vorticity and the magnitude of the cross-axial vorticity, respectively. Vorticity is concentrated near the axis in a round region with two spiral arms. The round region is mainly made of the axial vorticity, whereas the arms of the cross-axial vorticity. The core boundary shown in figure (d) deviates from a circle and the radius changes between 7λ and 9λ. Figure (e) is an arrow representation of the cross-axial velocity vector field relative to the axis. They rotate around the axis counterclockwise, which confirms the existence of swirling motions. Another arrow representation is figure (f) for the cross-vorticity vector field which is compared with figure (c). The cross-axial vorticity is wrapping around the axis to make a spiral pattern of double layers of opposite sings of vorticity. This is reminiscent of Moore's spiral vortex mentioned above. The pressure takes a minimum at the axis by definition (figure (g)). The Laplacian of pressure shown in figure (h), on the other hand, takes large values around the axis and has a similar shape as the axial vorticity (figure (b)). Finally, in figure (i) we see that the energy dissipation is taking place at the cross-axial vorticity layers much more actively than around the core. The surrounding vortex layers are dynamically more important than the core at least in the energy dissipation process.

5 Statistics of Vortex Cores

In order to examine the dynamical importance of vortex tubes we investigate the physical characteristics of vortex cores. Since the numerical data of the position of the core periphery is stored, the grid points in cores can be easily marked. This enables us to sum up any physical quantities inside cores selectively, e.g. the volume $V_{\rm core}$ occupied by the vortex cores, the contributions of the core to the enstrophy $Q_{\rm core}$ and the energy dissipation $\epsilon_{\rm core}$. In table 2, we list their values as the ratio to the contributions from the total volume V, the enstrophy Q and the energy dissipation ϵ, together with the mean axial vorticity $\omega_\parallel$, the mean core radius $R_{\rm core}$ and the mean circulation Γ for the three cases of different Reynolds numbers.

The Reynolds number dependence of core characteristics is important to infer the dynamical roles of vortices in the large Reynolds number limit. From this table the following Reynolds number dependence is found within statistical uncertainty (see figures 6 and 3).

$$V_{\rm core} \propto {R_\lambda}^{-(1.0\sim0.7)}, \tag{3}$$

$$\frac{\Gamma}{\nu} \propto {R_\lambda}^{-(1.2\sim1.3)}, \tag{4}$$

$$\frac{R_{\rm core}}{l_K} \propto {R_\lambda}^{-(0.6\sim1.0)}. \tag{5}$$

This behavior is quite different from that obtained by Jiménez & Wray (1998) [1]:

$$V_{\rm core} \propto {R_\lambda}^{-2}, \tag{6}$$

$$\frac{\Gamma}{\nu} \propto {R_\lambda}^{0.5}, \tag{7}$$

$$\frac{R_{\rm core}}{l_K} \propto {R_\lambda}^{0}. \tag{8}$$

Our vortex Reynolds number Γ/ν decreases with R_λ while theirs increases, our core radius decreases more rapidly than l_K and our

volume $V_{\rm core}$ decreases more slowly. In other words, our vortex tubes are thinner, longer and weaker than theirs. A possible reason of this difference is that their definition of core is different from ours. They compare the vorticity of a vortex core with an axi-symmetric Gaussian distribution and introduce the e^{-1} radius. They take the statistics of stronger vortices, whereas the vorticity magnitude is irrelevant for ours.

The probability density functions (PDF) of the core radius and the vortex Reynolds number are shown in figures 7 and 8, respectively. The scale similarity of these functions does not hold.

As seen in table 2, the vortex core occupies 13 $\sim$ 22% of the whole flow field which decreases as R_λ increases. The contributions of the core to the enstrophy and the energy dissipation are 36 $\sim$ 46% and 14 $\sim$ 19% of the total, respectively, which also decrease as R_λ increases. This suggests that the vortex tubes may become dynamically less important as the Reynolds number increases. On the other hand, as seen in figure 5(i), the energy dissipation is taking place more actively in the surrounding vortex layers which are well outside of the cores, beyond $2R_{\rm core}$, say. Therefore, the neighboring outside of the core can be more dynamically important.

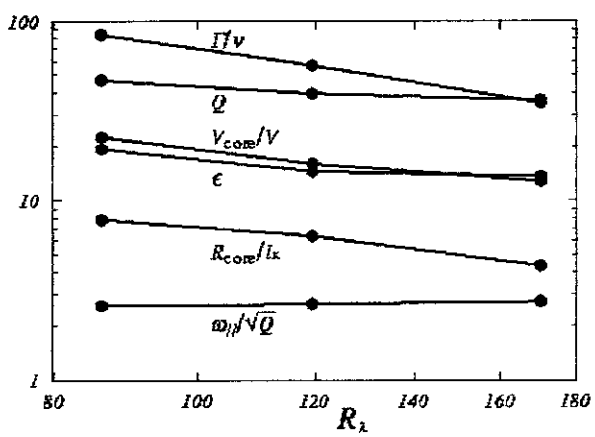

Figure 6: Reynolds number dependence of various physical quantities.

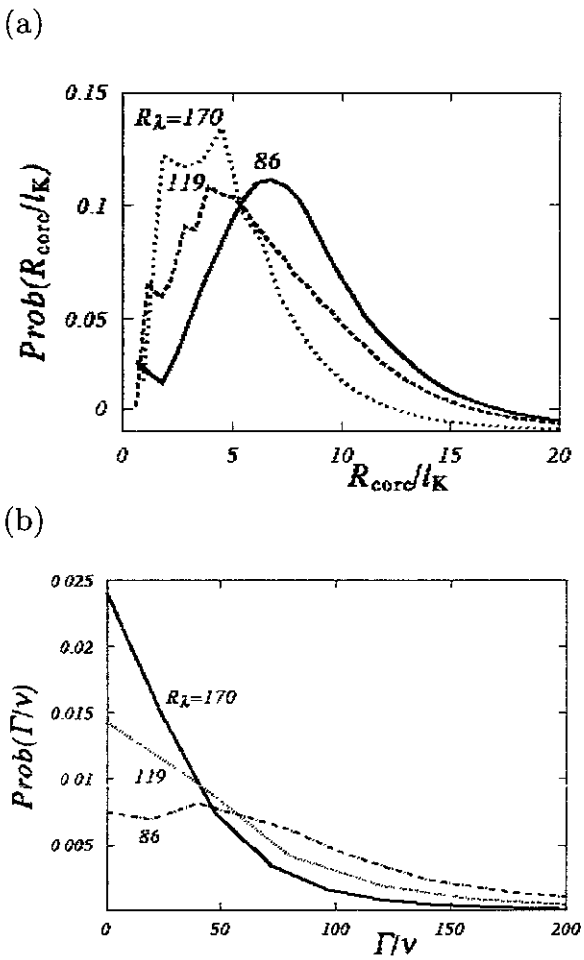

Figure 7: The PDF of (a) core radius and (b) circulation.

At the beginning of this section we marked the grid points inside cores and calculated the core volume and the contribution of the vortex core to various physical quantities. Similarly, by marking those grid points that are within some multiples of core radius. we can calculate the contribution from the regions within distance of the core radius times these multiples. The core contributions to the enstrophy and the energy dissipation thus obtained are shown in figure 8 for $R_\lambda = 86$. Here, the number attached to a point denotes the multiple. The abscissa represents the relative volume occupied by the vortex cores.

Although the vortex cores occupy only 22% of the volume, the regions within double and triple of the core radius from axes

include 70% and 93%. The contribution to the enstrophy from the core is 46%, which means that the enstrophy density is larger inside core than outside. The contribution to the energy dissipation is nearly proportional to the occupied volume though a small dip is recognized inside core. In view that the surrounding vortex layers are located around double the core radius, the contribution of these layers to the energy dissipation can be understood.

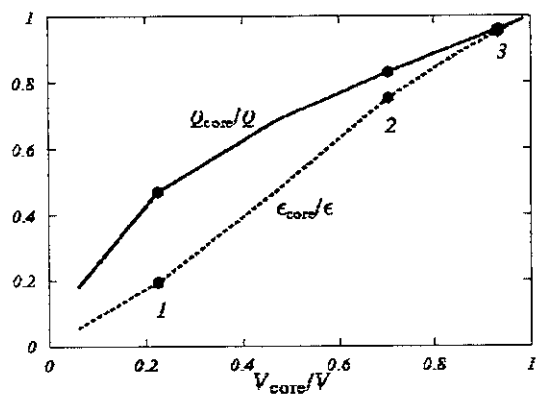

Figure 8: Contributions to the enstrophy and the energy dissipation rate of vortex core. The numbers show the multiple of core radius.

6 Concluding Remarks

The low-pressure-vortex visualization method has been applied to numerical box turbulence to discover that swirling tubular vortices, which had been known to appear ubiquitously in various kinds of turbulence, are always accompanied with winding vortex layers of cross-axial vorticity around them. The energy dissipation is taking place more actively in these vortex layers than in the tube part. The combination of the vortex tube and surrounding vortex layers, which may be called an *elementary vortex*, seems to be the fundamental coherent structure of turbulence. As the Reynolds number increases, will it be dynamically more important or be destroyed at all by some instabilities ? This is an interesting future problem.

References

[1] Jiménez, J. and Wray, A. A. (1998) "On the Characteristics of Vortex Filaments in Isotropic Turbulence." J. Fluid Mech. **373**, 255–285.

[2] Kawahara, G., Kida, S., Tanaka, M. and Yanase, S. (1997). "Wrap, Tilt and Stretch of Vorticity Lines around a Strong Thin Straight Vortex Tube in a Simple Shear Flow," J. Fluid Mech. **353**, 115-162.

[3] Kida, S. (2000). "Computational Analysis of Turbulence · Description by Low-Pressure Vortex," (submitted to Proc. ICIAM99).

[4] Kida, S. and Miura, H. (1998a). "Identification and Analysis of Vortical Structures," European Journal of Mechanics B/Fluids **17**, 471–488.

[5] Kida, S. and Miura, H. (1998b). "Swirl Condition in Low-Pressure Vortices," J. Phys. Soc. Japan, **67**, 2166-2169.

[6] Kida, S. and Miura, H. (2000). "Double Spirals around a Tubular Vortex in Turbulence," J. Phys. Soc. Japan (in press).

[7] Miura, H. and Kida, S. (1997). "Identification of Tubular Vortices in Turbulence," J. Phys. Soc. Japan, **66**, 1331–1334.

[8] Moore, D. W. (1985). "The Interaction of a Diffusing Line Vortex and Aligned Shear Flow," Proc. Roy. Soc. Lond. A **399**, 367–375.

Recent Issues of NIFS Series

NIFS-656 K Narihara, I Yamada, N Ohyabu, K Y Watanabe, N Ashikawa, P C deVries, M Emoto, H Funaba, M Goto, K Ichiguchi, K Ida, H Idei, K Ikeda, S Inagaki, N Inoue, K Isobe, S Kado, O Kaneko, K Kawahata, K Khlopenkov, TKobuchi, A Komori, S Kubo, R Kumazawa, Y Liang, TMasuzaki, TMinami, J Miyazawa, TMorisaki, S Morita, S Murakami, S Muto, T Mutoh, Y Nagayama, Y Nakamura, H Nakanishi, Y Narushima, K Nishimura, N Noda, T Notake, S Ohdachi, Y Oka, M Osakabe, S Ozaki, R O Pavlichenko, B.J Peterson, A Sagara, K Saito, S Sakakibara, R Sakamoto, H Sasao, M Sasao, K Sato, M Sato, TSeki, TShimozuma, C Shoji, H Suzuki, A Takayama, M Takechi, Y Takeiri, N Tamura, K Tanaka, K Toi, N Tokuzawa, Y Torii, K Tsumori, T Watari, H Yamada, S Yamaguchi, S Yamamoto, M Yokoyama, Y Yoshimura, S Satow, K Itoh, K Ohkubo, K Yamazaki, S Sudo, O Motojima, Y Hamada, M Fujiwara,
Transition from Ion Root to Electron Root in NBI Heated Plasmas in LHD Sep 2000
(IAEA-CN-77/EXP5/28)

NIFS-657 M Sasao, S Murakami, M Isobe, A V Krasilnikov, S Iiduka, K Itoh, N Nakajima, M Osakabe, K Saito,T Seki, Y Takeiri, T Watari, N Ashikawa , P deVaries, M Emoto, H Funaba, M Goto, K Ida, H Idei, K Ikeda, S Inagaki, N Inoue, S.Kado, O Kaneko, K Kawahata, K.Khlopenkov, TKobuchi , A.Komori, S Kubo, R Kumazawa, S Masuzaki, TMinami, J Miyazawa, TMorisaki, S Morita, S Muto, TMutoh, Y Nagayama, YNakamura, H Nakanishi, K Narihara, K Nishimura, N Noda, TNotake, YLiang , S Ohdachi, N Ohyabu, Y Oka, TOzaki, R O Pavlichenko, B J Peterson, A Sagara, S Sakakibara, R Sakamoto, H Sasao4, K Sato, M Sato, TShimozuma, M Shoji, H Suzuki, M Takechi, N Tamura, K Tanaka, K Toi, TTokuzawa, Y Torii, K Tsumori, H Yamada, I Yamada, S Yamaguchi, S Yamamoto, M Yokoyama, Y Yoshimura, K Y Watanabe and O. Motojima,
Study of Energetic Ion Transport in the Large Helical Device Sep 2000
(IAEA-CN-77/EX9/1)

NIFS-658 B J Peterson, Y Nakamura, K Yamazaki, N Noda, J Rice, Y Takeiri, M Goto, K Narihara, K Tanaka, K Sato, S Masuzaki, S Sakakibara, K Ida, H Funaba, M Shoji, M Osakabe, M Sato, Yuhong Xu, TKobuchi, N Ashikawa, P deVries, M Emoto, H Idei, K Ikeda, S Inagaki, N Inoue, M Isobe, S Kado, K Khlopenkov, S Kubo, R Kumazawa, TMinami, J Miyazawa, TMorisaki, S Murakami, S Muto, TMutoh Y.Nagayama, H Nakanishi, K Nishimura, TNotake, YLiang, S Ohdachi, YOka, TOzaki, R O Pavlichenko, A Sagara, K Saito, R Sakamoto, H Sasao, M Sasao TSeki, TShimozuma, H Suzuki, M Takechi, N.Tamura, K Toi TTokuzawa, Y Torii, K.Tsumori, I Yamada, S Yamaguchi, S Yamamoto, M.Yokoyama Y Yoshimura, K Y Watanabe, T Watari, K Kawahata, O Kaneko, N Ohyabu, H Yamada, A Komori, S Sudo, O Motojima
Impurity transport induced oscillations in LHD Sep 2000
(IAEA-CN-77/EXP5/27)

NIFS-659 T Satow, S Imagawa, N Yanagi, K Takahata, T Mito, S Yamada, H Chikaraishi, A Nishimura, I Ohtake, Y Nakamura, S Satoh, O Motojima,
Achieved Capability of the Superconducting Magnet system for the Large Helical Device Sep 2000
(IAEA-CN-77/FTP1/15)

NIFS-660 T Watari, T Mutoh, R Kumazawa, T Seki, K Saito, Y Torii, Y P Zhao, D Hartmann , H Idei, S Kubo, K Ohkubo, M Sato, T Shimozuma, Y Yoshimura, K Ikeda, O Kaneko, Y Oka, M Osakabe, Y Takeiri, K Tsumori, N Ashikawa , P.C deVries, M Emoto, A Fukuyama , H Funaba, M Goto, K. Ida, S Inagaki, N Inoue, M Isobe, K Itoh, S Kado, K Kawahata, T Kobuchi, K Khlopenkov, A Komori, A Krasilnikov , YLiang,S Masuzaki, K Matsuoka, T Minami, J Miyazawa, T Morisaki, S Morita, S Murakami, S Muto, Y Nagayama, Y Nakamura, H Nakanishi, K Narihara, K Nishimura, N Noda, A TNotake, S Ohdachi, N Ohyabu, H Okada , M Okamoto, T Ozaki, R O Pavlichenko, B J Peterson, A Sagara, S Sakakibara, R Sakamoto, H Sasao, M Sasao, K Sato, S Satoh, T Satow, M Shoji, S Sudo, H Suzuki, M Takechi, N Tamura ,S Tanahashi, K Tanaka, K Toi, T Tokuzawa, K Y Watanabe, T Watanabe H Yamada, I Yamada, S Yamaguchi, S Yamamoto, K Yamazaki, M Yokoyama, Y Hamada, O Motojima, M Fujiwara,
The Performance of ICRF Heated Plasmas in LHD Sep 2000
(IAEA-CN-77/EX8/4)

NIFS-661 K Yamazaki, K Y Watanabe, A Sagara, H Yamada, S Sakakibara, K Narihara, K Tanaka, M Osakabe, K Nishimura, O. Motojima, M Fujiwara, the LHD Group,
Helical Reactor Design Studies Based on New Confinement Scalings Sep 2000
(IAEA-CN-77/ FTP 2/12)

NIFS-662 T Hayashi, N Mizuguchi, H Miura and T Sato,
Dynamics of Relaxation Phenomena in Spherical Tokamak Sep 2000
(IAEA-CN-77THP2/13)

NIFS-663 H Nakamura and T Sato, H Kambe and K Sawada and T Saiki,
Design and Optimization of Tapered Structure of Near-field Fiber Probe Based on FDTD Simulation Oct 2000

NIFS-664 N Nakajima
Three Dimensional Ideal MHD Stability Analysis in $L=2$ Heliotron Systems Oct 2000

NIFS-665 S Fujiwara and T Sato,
Structure Formation of a Single Polymer Chain I Growth of trans Domains Nov 2000

NIFS-666 S Kida,
Vortical Structure of Turbulence Nov 2000